J. Cent. South Univ. (2022) 29: 1749−1760
DOI: https://doi.org/10.1007/s11771-022-5059-9

Springer

Siderite pyrolysis in suspension roasting: An in-situ study on kinetics, phase transformation, and product properties

ZHANG Qi(张琦)[1, 3], SUN Yong-sheng(孙永升)[1, 2, 3]*, QIN Yong-hong(秦永红)[1, 3], GAO Peng(高鹏)[1, 2, 3], YUAN Shuai(袁帅)[1, 3]

1. School of Resources and Civil Engineering, Northeastern University, Shenyang 110819, China;
2. State Key Laboratory of Rolling and Automation, Northeastern University, Shenyang 110819, China;
3. National-local Joint Engineering Research Center of High-efficient Exploitation Technology for Refractory Iron Ore Resources, Shenyang 110819, China

Abstract: Siderite, as an abundant iron ore, has not been effectively utilized, with a low utilization rate. In this study, the in-situ kinetics and mechanism of siderite during suspension magnetization roasting (SMR) were investigated to improve the selective conversion of siderite to magnetite and CO, enriching the theoretical system of green SMR using siderite as a reductant. According to the gas products analyses, the peak value of the reaction rate increased with increasing temperature, and its curves presented the feature of an early peak and long tail. The mechanism function of the siderite pyrolysis was the contraction sphere model (R_3): $f(\alpha)=3(1-\alpha)^{2/3}$; E_α was 46.4653 kJ/mol; A was 0.5938 s^{-1}; the kinetics equation was $k=0.5938\exp[-46.4653/(RT)]$. The in-situ HT-XRD results indicated that siderite was converted into magnetite and wüstite that exhibited a good crystallinity in SMR under a N_2 atmosphere. At 620 °C, the saturation magnetization (M_s), remanence magnetization (M_r), and coercivity (H_c) of the product peaked at 53.63×10^{-3} A·m^2/g, 10.23×10^{-3} A·m^2/g, and 12.40×10^3 A/m, respectively. Meanwhile, the initial particles with a smooth surface were transformed into particles with a porous and loose structure in the roasting process, which would contribute to reducing the grinding cost.

Key words: siderite; suspension magnetization roasting; reaction kinetics; phase transformation; magnetic transition; microstructure evolution

Cite this article as: ZHANG Qi, SUN Yong-sheng, QIN Yong-hong, GAO Peng, YUAN Shuai. Siderite pyrolysis in suspension roasting: An in-situ study on kinetics, phase transformation, and product properties [J]. Journal of Central South University, 2022, 29(6): 1749−1760. DOI: https://doi.org/10.1007/s11771-022-5059-9.

1 Introduction

Siderite ($FeCO_3$) is a widespread carbonate iron mineral, with proven reserves of 1.83 billion tons in China [1]. However, there are still more than 1.65 billion tons of siderite that remains unexploited [2−3]. With the increasing depletion of high-quality iron ore, the efficient production of siderite is significant for alleviating the shortage of iron ore in China. Siderite has the characteristics of low grade and easy argillization [4], which makes it difficult to obtain high-quality iron concentrates using conventional beneficiation techniques, such

Foundation item: Projects(51874071, 52022019, 51734005) supported by the National Natural Science Foundation of China; Project (161045) supported by the Fok Ying Tung Education Foundation for Yong Teachers in the Higher Education Institutions of China

Received date: 2021-05-31; **Accepted date:** 2021-12-21

Corresponding author: SUN Yong-sheng, PhD, Professor; Tel: +86-13504999754; E-mail: yongshengsun@mail.neu.edu.cn; ORCID: https://orcid.org/0000-0002-2419-1070

as gravity separation, magnetic separation, and flotation [5−7]. Therefore, based on the characteristics of siderite, magnetization roasting remains to be one of the most efficient technologies for the development of siderite [8]. Among them, suspension magnetization roasting (SMR) technology is an advanced technology developed independently by Northeastern University. Currently, the SMR has been popularized and applied in China Jiuquan Iron and Steel Co., Ltd. (iron ore project, 1.65 Mt/a) and Zambia (ferromanganese ore project, 0.60 Mt/a). As shown in Tables 1 and 2, compared with the traditional separation and magnetization roasting technologies, SMR technology has the characteristics of energy-saving, high efficiency, and stable product quality [9−13].

The pyrolysis products of siderite are closely related to the roasting atmosphere. The final pyrolysis products of siderite are α-Fe_2O_3 under an oxidizing atmosphere, Fe_3O_4 and FeO under a vacuum or inert atmosphere, and Fe_3O_4 under a CO_2 atmosphere [14 − 15]. Our previous study showed that siderite pyrolysis generates a large amount of CO (the maximum volume fraction of 15.88%) in an inert nitrogen atmosphere [16]. Therefore, SUN et al [17] proposed the suspension self-magnetization roasting process to roast the mixed samples of the siderite and hematite, achieving efficient recovery of iron minerals. And the reaction mechanism of self-magnetization roasting was studied (Figure 1) [18]. The suspension self-magnetization roasting provides a new way for the efficient and clean utilization of siderite ore.

Compared with the traditional roasting, the sufficient gas-solid contact and uniform siderite and temperature distribution in the SMR reactor will improve the pyrolysis rate and roasted product quality of siderite [11, 19]. To guide the green and clean SMR using siderite as a reductant, a systematic study of kinetics, phase transition, and product characteristics of siderite pyrolysis is necessary. Although scholars have conducted extensive experimental research on siderite pyrolysis kinetics in recent decades, most of the research adopted the thermal gravimetric analysis and the magnetite formation rate to solve the siderite pyrolysis kinetics in the non-in situ or static roasting [15, 20 − 23]. In comparison, the kinetic parameters obtained by real-time acquisition and analysis of gas-phase components during the SMR test using an infrared gas analyzer are closer to the intrinsic reaction characteristics [24−26].

In this study, based on the optimized conditions of self-magnetization roasting in our previous studies [16−18], the pyrolysis behavior of siderite in SMR was explored in terms of gas and solid products. It focused on the thermodynamics, components of tail gas, phase transition, magnetic transition, and microstructure evolution during siderite pyrolysis. The gas-phase products and phase transition during siderite pyrolysis in SMR were analyzed continuously by the infrared gas analyzer (IRGA) and in-situ high-temperature X-ray

Table 1 Comparison of main test indexes (%)

Iron ore	Traditional separation technology		SMR technology	
	Grade	Recovery	Grade	Recovery
JASCO lump ore	59−60	76−78	60−61	90−92
JASCO fine ore	44−46	64−66	59−62	85−87
JASCO tailings	20−22	—	58−60	57−59
Donganshan iron ore	65−66	63−65	66−67	88−90
Ansteel tailings	10−12	—	65−66	55−57
Shandong iron ore	55−56	—	64−65	95−97
Hainan iron ore	62−63	64−65	65−66	85−86

Table 2 Comparison of main parameters of different technologies

Technology	Feed size/mm	Recovery rate/%	Energy consumption/(GJ·t^{-1})	Productivity	Quality
Shaft furnace	15−75	70	1.2−1.4	Low productivity	Non-uniform quality
Rotary-kiln	0−25	75	1.8−2.1	Low productivity	Non-uniform quality
SMR	0−0.5	>85	0.9−1.2	High productivity	Uniform quality

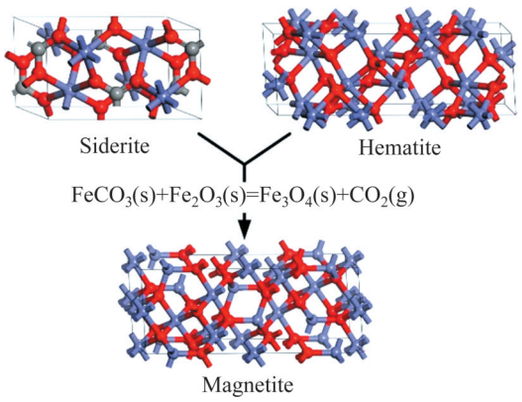

Figure 1 Mechanism of self-magnetization roasting of siderite and hematite

diffraction (in-situ HT-XRD), respectively. Furthermore, the suspension pyrolysis kinetics during siderite pyrolysis was explored.

2 Materials and methods

2.1 Materials

The siderite samples were obtained from Guangdong Province, China, and were ground until 70% of the particles passed sieve pore of 45 μm, as shown in Figure 2(a).

The main chemical and iron phase compositions of the siderite samples are listed in Tables 3 and 4, respectively, and XRD pattern is shown in Figure 2(b). The contents of TFe and FeO were 44.23% and 51.85%, respectively. Fe in the samples mainly existed in the form of siderite.

2.2 Apparatus and procedure

As shown in Figure 3, this roasting test system consists of a gas supply system, a suspended shaft tube, a temperature controller, and an infrared gas analyzer. The pyrolysis of siderite in a nitrogen atmosphere was carried out in the following order [16]: 1) Nitrogen (flow rate: 0.7 L/min, purity: 99.99%) was pumped into the system, and the furnace was raised to the test temperature at a heating rate of 15 °C/min. 2) Then, 3.00 g of samples were placed in the perforated quartz plate. And changes in gaseous product components were monitored and recorded in real-time. 3) After the reaction, the sample was cooled to room temperature (25 °C) in a nitrogen atmosphere, and the characteristics of the products were further analyzed.

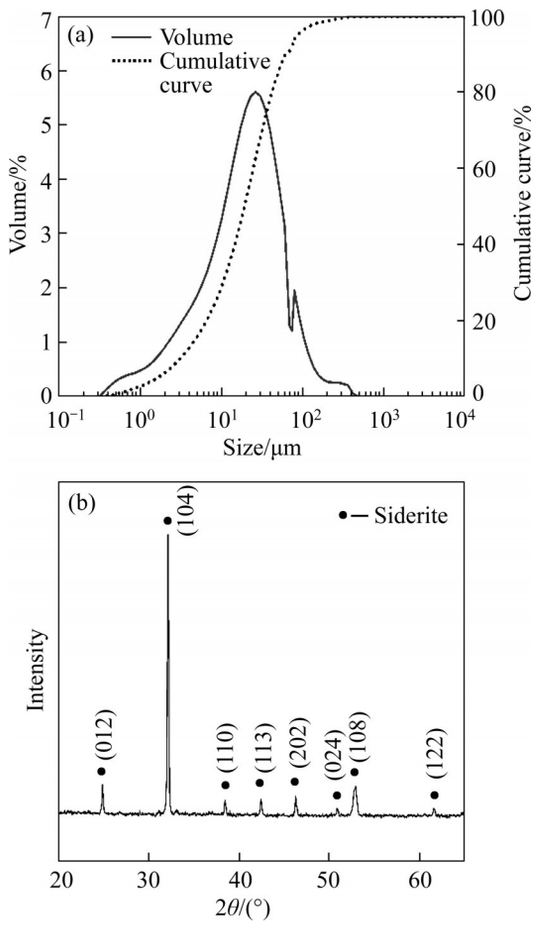

Figure 2 (a) Size distribution curve and (b) XRD pattern of siderite sample

Table 3 Major chemical composition analysis of siderite sample (wt%)

TFe	FeO	SiO_2	MgO	CaO
44.23	51.85	0.38	1.22	0.35
Al_2O_3	Mn	P	S	LOI
0.14	2.66	<0.005	1.5	36.74

Table 4 Iron phase composition of siderite sample

Iron phase	*w*/%	Distribution/%
Fe in carbonate	42.16	95.32
Fe in magnetite	0.41	0.93
Fe in hematite	1.51	3.41
Fe in sulfide	0.10	0.23
Fe in silicate	0.05	0.11
TFe	44.23	100.00

2.3 Products characterization

The chemical compositions of the siderite sample are determined by chemical methods

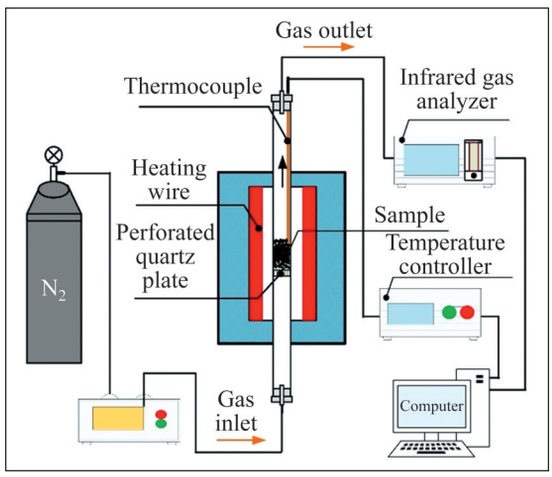

Figure 3 Schematic diagram of experimental system of suspension roasting

combined with X-ray fluoroscopy. The iron phase of the sample was analyzed by the iron chemical phase analysis method [28]. The particle size of the sample was measured with a laser particle size analyzer (LPSA, MS2000). The phase of sample was investigated by X-ray diffraction (XRD, PW3040). The in-situ phase transformation of the siderite pyrolysis was studied by in-situ high-temperature HT-XRD (Smart Lab 9 kW) with Cu K_α radiation and 40 ° C/min heating rate. The VSM (JDAW-2000D, LAKESHORE) was used to analyze the magnetic property of the roasted samples. The micromorphology of the samples was investigated using SEM (ULTRA PLUS, Zeiss).

The concentrations of gaseous components were analyzed and recorded in real-time using an infrared gas analyzer (Gasboaed-3100, Cubic-Ruiyi). The reaction fraction (α) and reaction rate (v) of the pyrolysis reaction are as follows:

$$\alpha=\frac{V_t}{V_{t_n}}=\frac{\sum_0^t(C_tQ_t\Delta t)}{\sum_0^{t_n}(C_tQ_t\Delta t)} \tag{1}$$

$$v=\frac{\mathrm{d}\alpha}{\mathrm{d}t}=\frac{C_tQ_t\Delta t}{\sum_0^{t_n}(C_tQ_t\Delta t)} \tag{2}$$

where α is the reaction fraction; t_n is the reaction completion time, s; V_t is the cumulative amount of gas at reaction time t, L; V_{t_n} is the cumulative amount of gas at the completed reaction, L; C_t is the gas concentration at reaction time t, %; Q_t is the gas flow at reaction time t, L/min; v is the reaction rate, s^{-1}.

2.4 Kinetics modeling

The kinetics equations of the isothermal reaction are shown in Eqs. (3)−(5):

$$\mathrm{d}\alpha/\mathrm{d}t=k(T)f(\alpha) \tag{3}$$

$$k(T)=A\exp[-E_a/(RT)] \tag{4}$$

$$\ln k=\ln A-E_a/(RT) \tag{5}$$

where $k(T)$ is the kinetic rate constant, s^{-1}, which can be expressed as Eq. (4); $f(\alpha)$ is the mechanism function of the reaction model [13, 18]; R is the gas constant, 8.314 J/(mol·K); A is the pre-exponential factor, s^{-1}; E_a is the apparent activation energy, J/mol; and T is the reaction temperature, K.

Linear fitting was performed for the test data to obtain the correlation coefficient (R^2) of the mechanism function. Based on the common pyrolysis reaction models, the function expression of $f(\alpha)$ with the highest linear correlation was determined to be the optimal mechanism function by the model matching method [14, 27−29]. In this study, $k(T)$ at varying temperatures (510, 560, 620, 670 and 720 °C) was adopted to investigate E_a and A of the siderite pyrolysis reaction [30].

3 Results and discussion

3.1 Thermodynamic calculations

The thermodynamic calculation results of Eqs. (6)−(8) in the range of 0−800 °C are plotted in Figure 4.

$$\mathrm{FeCO_3(s)=FeO(s)+CO_2(g)} \tag{6}$$

$$\mathrm{FeO(s)+1/3CO_2(g)\rightleftharpoons 1/3Fe_3O_4(s)+1/3CO(g)} \tag{7}$$

$$\mathrm{FeCO_3(s)=1/3Fe_3O_4(s)+2/3\ CO_2(g)+1/3CO(g)} \tag{8}$$

The ΔG^Θ values of Eqs. (6) and (8) are negative when the roasting temperature exceeds 167 °C (Figure 4(a)). This shows that the pyrolysis reaction of siderite can proceed spontaneously under the test conditions. Moreover, increasing the temperature favors the pyrolysis reaction of siderite. The reaction of Eq. (7) is exothermic, and

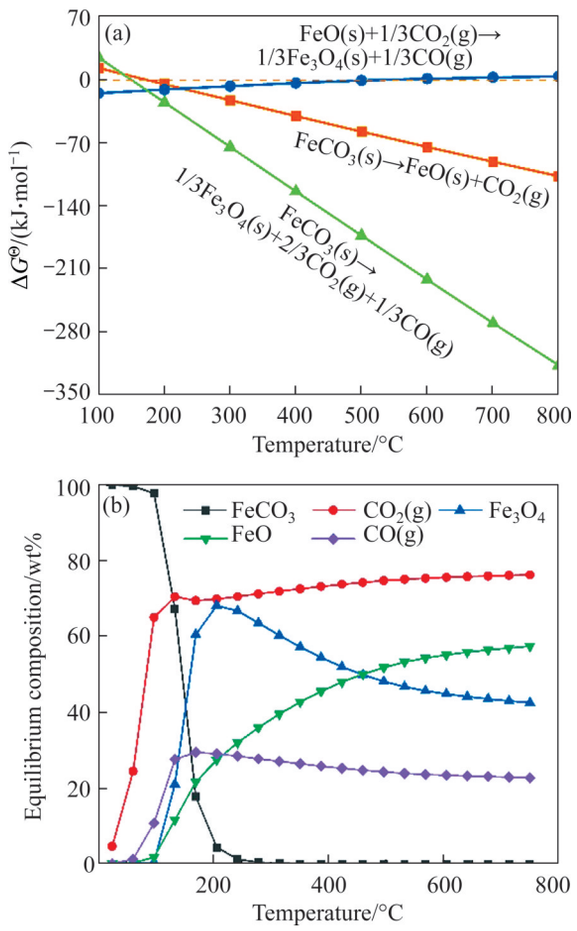

Figure 4 (a) Dependence of Gibbs free energy on temperature; (b) Equilibrium compositions of siderite pyrolysis

increasing the temperature will drive the reaction equilibrium to the left, which does not favor the generation of magnetite.

Figure 4(b) shows that the increase in temperature promotes the pyrolysis of siderite and increases the conversion of pyrolysis. Wüstite (FeO) is an intermediate product of the conversion of siderite to magnetite. The increase in temperature drives the equilibrium of Eq. (7) to the left, resulting in a decrease in the conversion of the reaction.

In addition, CO_2 concentration also has an important effect on the equilibrium (Eq. (7)), and the increase in CO_2 concentration drives the equilibrium to the right, which is favorable for increasing the conversion of Eq. (7) [16]. Therefore, the CO_2 generated by CO reduction of hematite can also promote the conversion of siderite pyrolysis products (FeO) to magnetite in the process of self-magnetization roasting.

3.2 Tail gas analyses

The roasting temperature had a significant influence on the pyrolysis rate of siderite. As the roasting temperature increased from 510 °C to 720 °C, the peak value of the CO_2 flow rate gradually increased from 11.54 mL/min to 114.67 mL/min. Namely, the reaction rate (v) of the siderite pyrolysis increased as the temperature increased (Figure 5(a)). Because the apparent activation energy (E_a) of the siderite pyrolysis reaction is always positive [14, 21, 31], the reaction rate constant (k) increases as the temperature increases. Similar to the flow curve of CO_2, the peak value of the CO flow curve increased with an increase in temperature, and the CO_2 and CO flow curves all showed the characteristics of "an early peak and a long tail" (Figure 5(b)). Figures 4(a) and (b) show that the flow curves of CO_2 and CO reach their peaks almost simultaneously at each temperature, indicating that the FeO magnetization reaction (Eq. (7)) and the pyrolysis reaction (Eqs. (6) and (8)) were carried out simultaneously.

3.3 Pyrolysis kinetics

Because the pyrolysis rate of siderite is proportional to the sum of the precipitation rates of CO_2 and CO in the tail gas simultaneously, the kinetic equations and parameters are solved by the sum of the precipitation rates of CO_2 and CO. The trends of the reaction fraction curves ($\alpha - t$) are similar at different temperatures (Figure 5(c)). With the increase in reaction time, the reaction fraction (α) shows a steep increase, then a slight increase, and finally tends to 1. The α increases as the temperature raises at the same reaction time. Notably, α increases from 0.09 (460 °C) to 0.87 (720 °C) in 250 s. Figure 5(d) demonstrates that the reaction rate increases as the pyrolysis temperature increases.

The most probable mechanism function of siderite pyrolysis, the formula of the $f(\alpha)$ function, was evaluated by comparing common mathematical models in Ref. [16]. The values of the linear R^2 for various kinetics models were calculated with α ranging from 0.1 to 0.9 (Table 5). The most probable mechanism function of the value reaction was determined according to the proximity of R^2 close to 1 [32]. The R^2 of various temperatures obtained by the phase boundary reaction model (R_3:

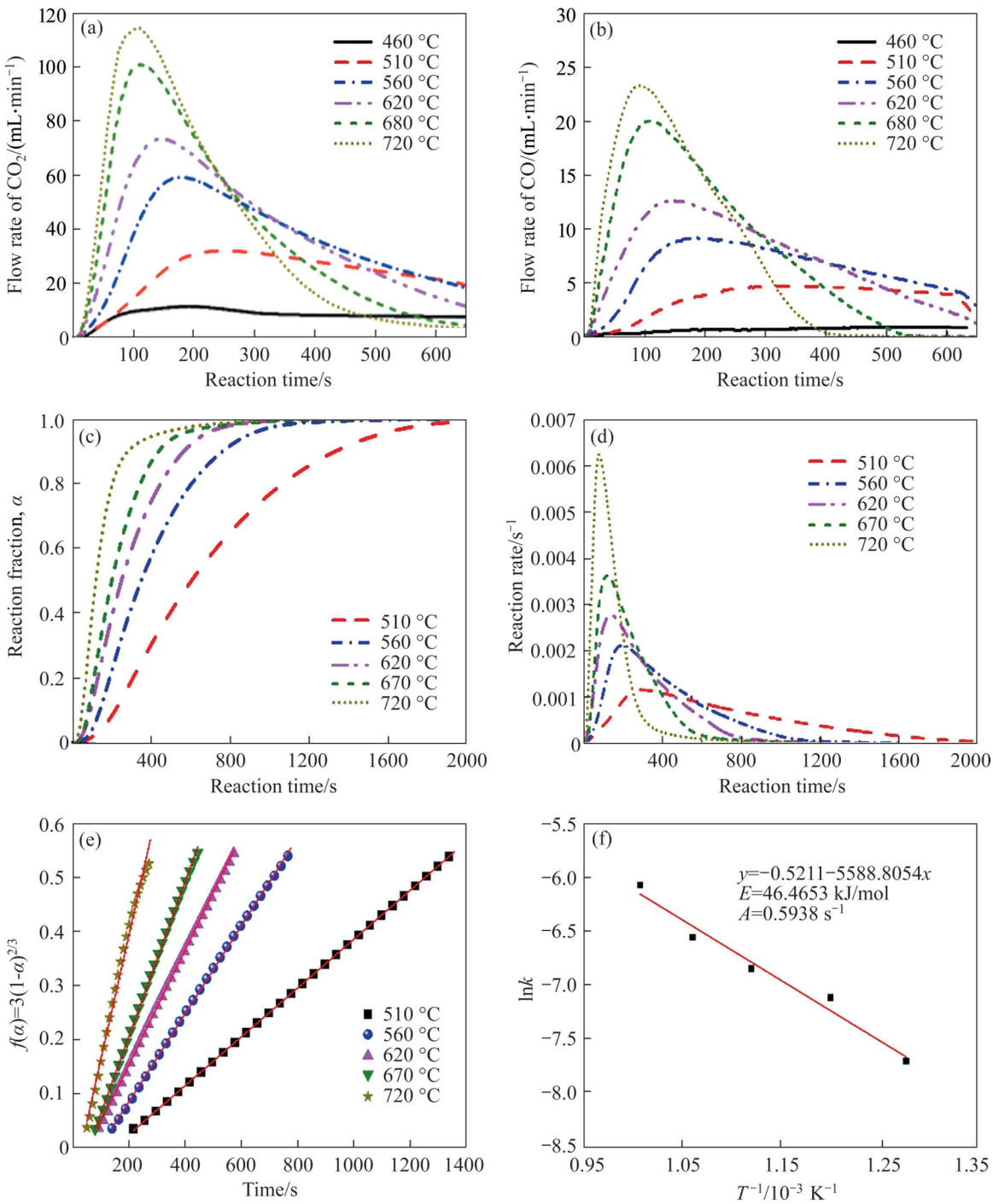

Figure 5 (a) CO_2 flow, (b) CO flow, (c) reaction fraction, and (d) reaction rate at different temperatures; (e) Linear fitting of $f(\alpha)=3(1-\alpha)^{2/3}$; (f) Linear fitting of ln$k$ versus 1/T

contraction sphere, n=3) was closer to 1 than the other models. The most probable mechanism function of the siderite pyrolysis reaction was the R_3 model (3D phase boundary contraction model): $f(\alpha)=3(1-\alpha)^{2/3}$ (Figure 5(e)).

According to Eqs. (4) and (5), the values of E_α, A, and k were calculated (Figure 5(f)), and the following data were obtained: E_α=46.4653 kJ/mol, A =0.5938 s^{-1}, and k=0.5938exp[−46.4653/(RT)]. So, the control type of siderite pyrolysis reaction belonged to the 3D phase boundary reaction of the chemical reaction ($E_{\text{chemical reaction}}$: 30−85 kJ/mol).

3.4 Phase transformation

As the roasted products contained a large amount of FeO, the wüstite phase (FeO) of the

Table 5 Correlation coefficients obtained by common reaction mechanism function [13, 18]

Reaction model	$f(\alpha)$	R^2					
		510 °C	560 °C	620 °C	670 °C	720 °C	Average
A_1	$1-\alpha$	0.9899	0.9610	0.9933	0.9938	0.9983	0.9873
$A_{3/2}$	$(3/2)(1-\alpha)[-\ln(1-\alpha)]^{1/2}$	0.9837	0.9811	0.9973	0.9894	0.9901	0.9883
A_2	$2(1-\alpha)[-\ln(1-\alpha)]^{1/2}$	0.9939	0.9922	0.9914	0.9915	0.9780	0.9894
A_3	$3(1-\alpha)[-\ln(1-\alpha)]^{2/3}$	0.9801	0.9770	0.9759	0.9756	0.9580	0.9733
A_4	$4(1-\alpha)[-\ln(1-\alpha)]^{3/4}$	0.9697	0.9660	0.9648	0.9644	0.9450	0.9620
P_1	$2\alpha^{1/2}$	0.9130	0.9053	0.9046	0.9030	0.8749	0.9002
R_1	1	0.9664	0.9604	0.9599	0.9587	0.9335	0.9558
R_2	$2(1-\alpha)^{1/2}$	0.9977	0.9959	0.9956	0.9951	0.9813	0.9931
R_3	$3(1-\alpha)^{2/3}$	1.0000	0.9997	0.9997	0.9995	0.9909	0.9979
D_1	$1/(2\alpha)$	0.9965	0.9956	0.9962	0.9948	0.9832	0.9933
D_2	$[-\ln(1-\alpha)]^{-1}$	0.9873	0.9902	0.9910	0.9904	0.9917	0.9901
D_3	$(3/2)(1-\alpha)^{2/3}/[1-(1-\alpha)^{1/3}]$	0.9471	0.9547	0.9558	0.9568	0.9789	0.9586
D_4	$(3/2)[(1-\alpha)^{-1/3}-1]^{-1}$	0.9771	0.9816	0.9825	0.9824	0.9904	0.9828
F_0	1	0.9664	0.9604	0.9599	0.9587	0.9335	0.9558
F_1	$1-\alpha$	0.9899	0.9610	0.9933	0.9938	0.9983	0.9873
F_2	$(1-\alpha)^2$	0.8526	0.8645	0.8673	0.8717	0.9287	0.8769

roasted products was easily oxidized to hematite or magnetite in air. And siderite with residual heat continued to pyrolyze during cooling. Therefore, the in-situ HT-XRD result was closer to the intrinsic characteristics of the phase transition. Because the same location of the material was tested in the in-situ HT-XRD analysis, the real-time information of the phase transition was accurately obtained during the siderite pyrolysis process.

In-situ HT-XRD patterns of the samples (Figure 6) reveal that the diffraction peaks of siderite appear at 2θ values of 25°, 32°, 38°, 42°, 46°, 51°, 53° and 62°, corresponding to the (012), (104), (110), (113), (202), (024), (018) and (122) lattice planes, respectively. This matches well with the standard siderite diffraction peaks. There was no significant change in the diffraction peak of the sample when the sample temperature was increased from 50 °C to 410 °C. When the temperature exceeded 410 °C, the diffraction peak intensity of the sample changed significantly. The intensity of the diffraction peaks of siderite decreased, while that of magnetite increased, indicating that siderite was gradually transformed to magnetite, as shown in Eq. (6) [33]. When the roasting temperature was 510 °C, the diffraction peaks of the magnetite were detected at 2θ values of 30°, 35°, 43°, 57° and 63°, corresponding to (220), (311), (400), (511) and (440) lattice planes, respectively [34−35]. Moreover, the diffraction peaks of wüstite were observed at 2θ values of 36°, 42° and 61° corresponding to (111), (200) and (220) lattice planes, respectively [36−38]. The intensity of the magnetite and wüstite diffraction peaks increased with an increase in temperature. This indicated that increasing the temperature favored the pyrolysis reaction of siderite, which was consistent with the analysis of the gaseous product. The diffraction peaks of siderite disappeared at 620 °C. It indicated that the siderite had been completely pyrolyzed and converted to magnetite and wüstite at 620 °C. When the temperature exceeded 620 °C, the intensity of the magnetite and wüstite diffraction peaks stabilized, indicating that the crystal shapes of magnetite and wüstite also tended to become perfected.

Only the diffraction peaks of magnetite and wüstite remained in the final product, indicating that it was a mixture of magnetite and wüstite. The result was consistent with the theoretical analysis in Section 3.1. Besides, the siderite pyrolysis produced a large amount of FeO and CO in N_2, so a large amount of reducing material was wasted by roasting siderite alone [16]. Therefore, it is feasible to

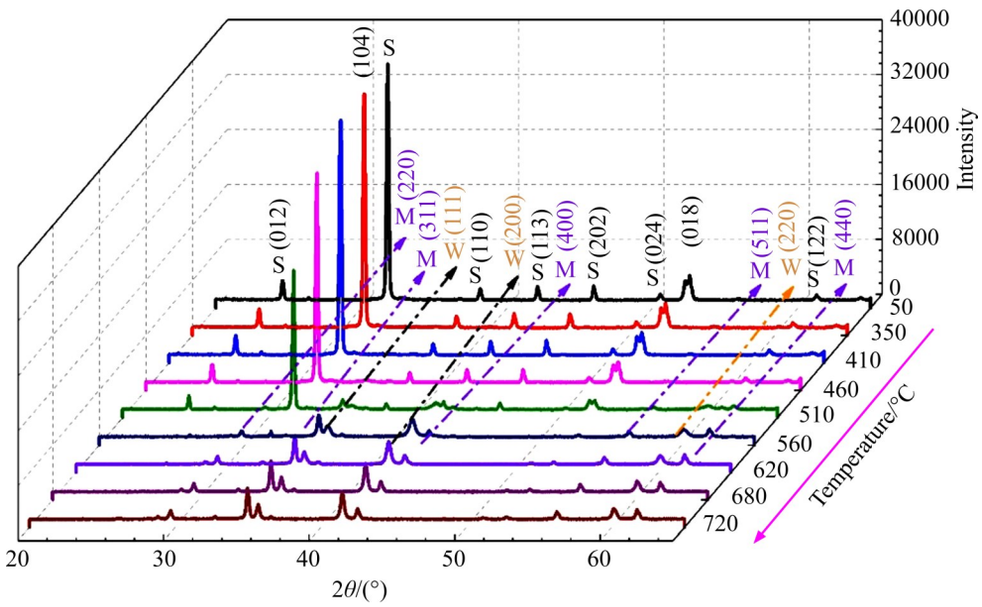

Figure 6 In situ HT-XRD patterns with 2θ range from 20° to 65°: S−siderite; M−magnetite; W−wüstite

decrease carbon emissions in self-magnetizing roasting using siderite instead of coal as a reductant [18].

3.5 Magnetic transition

The difference in magnetic properties between iron minerals and gangue minerals directly determines the enrichment effect of the iron minerals in the subsequent magnetic separation. Thus, it is important to study the magnetic properties of roasted products. As the temperature increased, the M_s of the roasted products showed a trend of first increasing to peak and then slowly decreasing (Figure 7(a)). The M_s of roasted products increased from 1.37×10^{-3} A·m^2/g at 50 °C to 53.63×10^{-3} A·m^2/g at 620 °C and peaked at 620 °C (Figure 7(b)). The essence of the magnetic increase was the conversion of weakly magnetic siderite to strongly magnetic magnetite [39]. The increase in temperature contributed to the increase in the pyrolysis rate of siderite (Eqs. (6) and (8)). But a too high temperature would inhibit the synthesis of magnetite (Eq. (7)), leading to a content decrease in strongly magnetic magnetite and a content increase in weakly magnetic wüstite, thus reducing the M_s of the samples. The phenomenon was consistent with the thermodynamic calculations and in situ HT-XRD analysis.

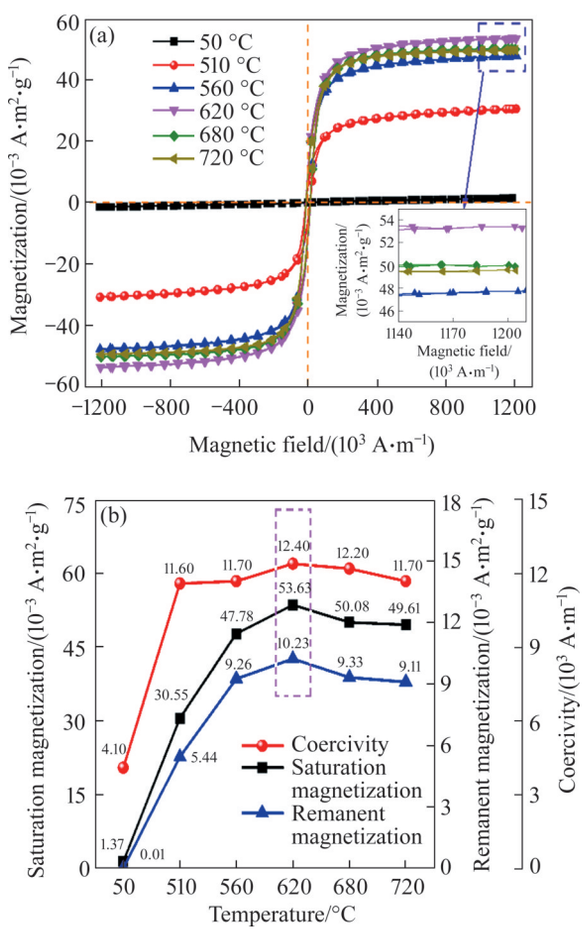

Figure 7 (a) Hysteresis loops for the roasted products; (b) Magnetic properties of the roasted products at different temperatures

As the pyrolysis temperature increased from 50 °C to 720 °C, the change law of coercivity (H_c) and remanence magnetization (M_r) was similar to that of M_s. The value of H_c and M_r increased from

4.10×10^3 A/m and 0.01×10^{-3} A·m^2/g at 50 °C to 12.40×10^3 A·m^2/g and 10.23×10^{-3} A·m^2/g at 620 °C in the roasted products. The crystal lattice parameters of the siderite were transformed by pyrolysis to generate internal stresses within the lattice. The presence of internal stresses increased the anisotropy and coercivity of the crystal [40]. Therefore, the coercive force of the roasted particles (510−720 °C) controlled by the local stress was greater than that of the initial particles (50 °C) [41−42].

From the gas analysis and in-situ HT-XRD analysis, the essence of the magnetic transition is the iron phase transition. At this initial stage of 510−620 °C, the magnetite content increased as the roasting temperature increased. However, when the temperature exceeded 620 °C, the reaction (Eq. (7)) was suppressed and the production of magnetite decreased [16].

3.6 Microstructure evolution

To further study the influence of SMR on siderite pyrolysis, the microstructures of the initial particles and the roasted particles (620 °C, 10 min) were observed via SEM-EDS, as shown in Figure 8. The initial particles had a smooth surface without pores (Figure 8(a)), and there were C, O, Mn and Fe elements on the surface (Figure 8(f)). After roasting, numerous pores appeared on the surface of the roasted particles, which were produced by the in-situ shrinkage of siderite particles and the release of gaseous products (CO_2 and CO) (Figures 8(b)−(d)). Meanwhile, the roasted particles after the in-situ contraction showed a near-spherical or neoplastic aggregate, exhibiting a 3D shrinkage morphology, and their microstructure conformed to the 3D contraction model (R_3).

During the pyrolysis of siderite particles, the gas was released from the inside to the outside. The thermal expansion of the gas also promoted the formation of pores and microcracks. The porous structure facilitated gas diffusion and siderite pyrolysis [16]. In addition, the diffraction peak of the C element disappeared and the diffraction peak intensity of the Fe element was enhanced (Figure 8(e)), which indicated that CO_2 was released during the pyrolysis process.

4 Conclusions

In this paper, the mechanism of the siderite pyrolysis during SMR was explored, with the emphasis on components of tail gas, in-situ kinetics, in-situ phase transition, magnetic transition, and microstructure evolution. The peak values of the reaction rate of siderite increased with the temperature rising, and its time was also advanced. The siderite pyrolysis was controlled by the phase boundary reaction of the 3D contraction sphere (R_3). The E_α was calculated to be 46.4653 kJ/mol; A was

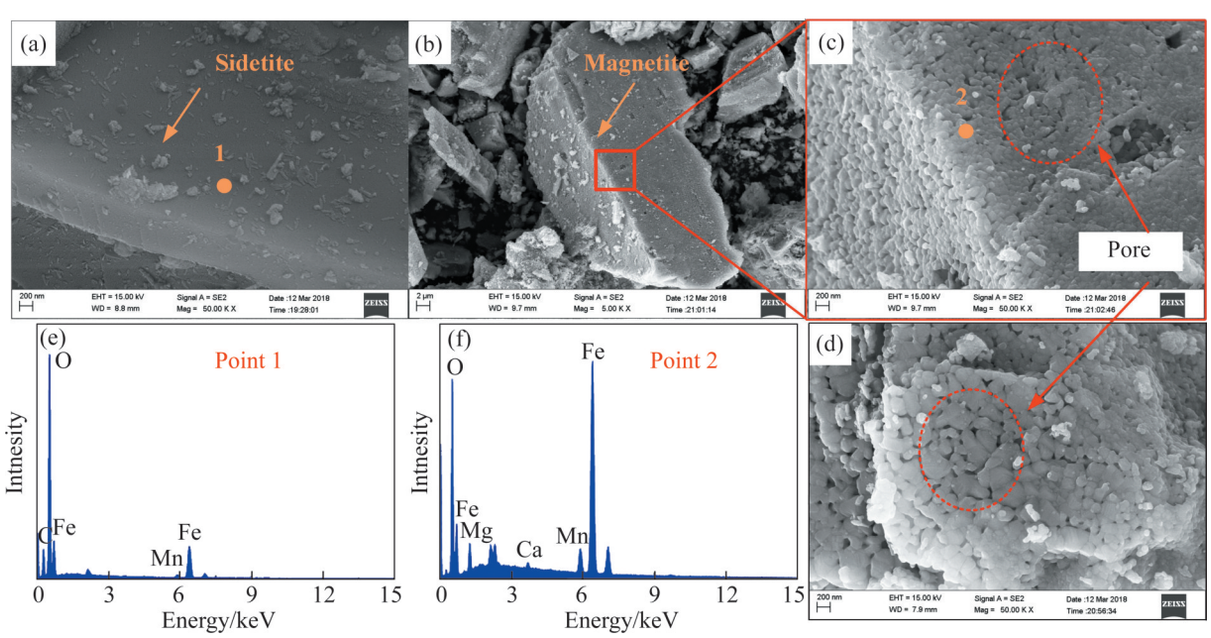

Figure 8 SEM of (a) initial sample particles and (b, c, d) roasted particles (620 °C, 10 min); EDS spectra of Point 1 (e) and Point 2 (f)

0.5938 s^{-1}; and the kinetics equation was k= 0.5938exp[−46.4653/(RT)]. The in-situ HT-XRD results indicated that the siderite pyrolyzed into magnetite and wüstite as the temperature exceeded 410 °C. And the final roasted product was the mixture of magnetite and wüstite in N_2. With an increase in roasting temperature, the values of the M_s, M_r and H_c of the roasted products gradually increased first, and then peaked at 620 °C for 53.63×10^{-3} A·m^2/g, 10.23×10^{-3} A·m^2/g and 12.40×10^3 A/m. Additionally, siderite pyrolysis produced numerous pores on the particle surface, which would promote gas diffusion and siderite pyrolysis.

Contributors

The overarching research goals were developed by ZHANG Qi and SUN Yong-sheng. ZHANG Qi provided measured data, analyzed the results, and edited the draft of the manuscript. SUN Yong-sheng provided the concept, conducted the literature review, and reviewed the manuscript. QIN Yong-hong, GAO Peng, and YUAN Shuai edited and revised the final version.

Conflict of interest

ZHANG Qi, SUN Yong-sheng, QIN Yong-hong, GAO Peng, and YUAN Shuai declare that they have no conflict of interest.

References

[1] CHEN Dong, GUO Hong-wei, LV Ya-nan, et al. Green technology-based utilization of refractory siderite ores to prepare electric arc furnace burden [J]. Steel Research International, 2021, 92(9): 2100046. DOI: 10.1002/srin.202100046.

[2] ZHANG Ying-chun, YANG Xiu-hong, SHI Ni-cheng, et al. Study on the comprehensive utilization of siderite [J]. Metal Mine, 2001, 295(1): 48−49, 53. (in Chinese)

[3] LUO Li-qun. Explerative research on beneficiation of siderite and its development prospect [J]. Metal Mine, 2006, 355 (1): 68−72. (in Chinese)

[4] ZHANG Chen, LI Li-xia, YUAN Zhi-tao, et al. Probing the effect of particle imperfections on the sliming of siderite in carbonate-bearing iron ore [J]. Minerals Engineering, 2019, 143: 106014. DOI: 10.1016/j.mineng.2019.106014.

[5] BAI Shao-jun, WEN Shu-ming, LIU Dian-wen, et al. Separation of phosphorus and magnetic mineral fines from siderite reductive ore by applying magnetic flocculation [J]. Separation Science and Technology, 2014, 49(9): 1434 − 1441. DOI: 10.1080/01496395.2013.877036.

[6] HAO Hai-qing, LI Li-xia, SOMASUNDARAN P, et al. Adsorption of pregelatinized starch for selective flocculation and flotation of fine siderite [J]. Langmuir, 2019, 35(21): 6878−6887. DOI: 10.1021/acs.langmuir.9b00669.

[7] YIN Wan-zhong, HAN Yue-xin, XIE Feng. Floatation separation research on siderite-containing iron concentrate [J]. Advanced Materials Research, 2010, 92: 103−109. DOI: 10.4028/www.scientific.net/amr.92.103.

[8] YU Jian-wen, HAN Yue-xin, LI Yan-jun, et al. Recent advances in magnetization roasting of refractory iron ores: A technological review in the past decade [J]. Mineral Processing and Extractive Metallurgy Review, 2020, 41(5): 349−359. DOI: 10.1080/08827508.2019.1634565.

[9] ZHANG Xiao-long, HAN Yue-xin, SUN Yong-sheng, et al. Innovative utilization of refractory iron ore via suspension magnetization roasting: A pilot-scale study [J]. Powder Technology, 2019, 352: 16 − 24. DOI: 10.1016/j.powtec.2019.04.042.

[10] SUN Yong-sheng, ZHANG Xiao-long, HAN Yue-xin, et al. A new approach for recovering iron from iron ore tailings using suspension magnetization roasting: A pilot-scale study [J]. Powder Technology, 2020, 361: 571 − 580. DOI: 10.1016/j.powtec.2019.11.076.

[11] TANG Zhi-dong, GAO Peng, LI Yan-jun, et al. Recovery of iron from hazardous tailings using fluidized roasting coupling technology [J]. Powder Technology, 2020, 361: 591−599. DOI: 10.1016/j.powtec.2019.11.074.

[12] TANG Zhi-dong, HAN Yue-xin, GAO Peng, et al. Fluidization characteristics of a U-type reduction chamber in a suspension roaster [J]. Powder Technology, 2019, 345: 64−73. DOI: 10.1016/j.powtec.2018.12.088.

[13] YUAN Shuai, ZHANG Qi, YIN Heng, et al. Efficient iron recovery from iron tailings using advanced suspension reduction technology: A study of reaction kinetics, phase transformation, and structure evolution [J]. Journal of Hazardous Materials, 2021, 404: 124067. DOI: 10.1016/j.jhazmat.2020.124067.

[14] ZHANG Xiao-long, HAN Yue-xin, LI Yan-jun, et al. Effect of heating rate on pyrolysis behavior and kinetic characteristics of siderite [J]. Minerals, 2017, 7(11): 211. DOI: 10.3390/min7110211.

[15] GOTOR F J, MACÍAS M, ORTEGA A, et al. Comparative study of the kinetics of the thermal decomposition of synthetic and natural siderite samples [J]. Physics and Chemistry of Minerals, 2000, 27(7): 495−503. DOI: 10.1007/s002690000093.

[16] ZHANG Qi, SUN Yong-sheng, HAN Yue-xin, et al. Pyrolysis behavior of a green and clean reductant for suspension magnetization roasting [J]. Journal of Cleaner Production, 2020, 268: 122173. DOI: 10.1016/j.jclepro.2020.122173.

[17] SUN Yong-sheng, ZHU Xin-ran, HAN Yue-xin, et al. Green magnetization roasting technology for refractory iron ore using siderite as a reductant [J]. Journal of Cleaner Production, 2019, 206: 40−50. DOI: 10.1016/j.jclepro.2018.09.113.

[18] ZHANG Qi, SUN Yong-sheng, HAN Yue-xin, et al. Producing magnetite concentrate via self-magnetization roasting in N_2 atmosphere: Phase and structure

transformation, and extraction kinetics [J]. Journal of Industrial and Engineering Chemistry, 2021, 104: 571−581. DOI: 10.1016/j.jiec.2021.09.008.

[19] HE Kun, ZHENG Zhong, CHEN Zhi-wei. Multistep reduction kinetics of Fe_3O_4 to Fe with CO in a micro fluidized bed reaction analyzer [J]. Powder Technology, 2020, 360: 1227−1236. DOI: 10.1016/j.powtec.2019.10.094.

[20] ZHAO Qiang, XUE Ji-lai, CHEN Wen. Mechanism of improved magnetizing roasting of siderite-hematite iron ore using a synergistic CO-H_2 mixture [J]. Journal of Iron and Steel Research International, 2020, 27(1): 12−21. DOI: 10.1007/s42243-019-00242-w.

[21] ALKAÇ D, ATALAY Ü. Kinetics of thermal decomposition of Hekimhan-Deveci siderite ore samples [J]. International Journal of Mineral Processing, 2008, 87(3−4): 120−128. DOI: 10.1016/j.minpro.2008.02.007.

[22] FENG Zhi-li, YU Yong-fu, LIU Gen-fan, et al. Kinetics of the thermal decomposition of wangjiatan siderite [J]. Journal of Wuhan University of Technology-Material Edition Science, 2011, 26(3): 523−526. DOI: 10.1007/s11595-011-0261-x.

[23] YU Da-wei, ZHU Ming-qian, UTIGARD T A, et al. TGA kinetic study on the hydrogen reduction of an iron nickel oxide [J]. Minerals Engineering, 2013, 54: 32−38. DOI: 10.1016/j.mineng.2013.03.018.

[24] ALVAREZ-AULAR A, CARTAYA L, MALDONADO A, et al. Experimental and DFT studies for the kinetics and mechanism of the pyrolysis of 2-(4-substituted-phenoxy) tetrahydro-2H-pyranes in the gas-phase [J]. Journal of Analytical and Applied Pyrolysis, 2018, 134: 52−60. DOI: 10.1016/j.jaap.2018.05.006.

[25] MONASCAL Y, GALLARDO E, CARTAYA L, et al. Homogeneous, unimolecular gas-phase pyrolysis kinetics of 4- and 2-hydroxyacetophenone [J]. Journal of Analytical and Applied Pyrolysis, 2017, 124: 499−503. DOI: 10.1016/j.jaap.2017.01.031.

[26] AL-QALLAF M A, DIB H H, AL-AWADI N A, et al. Arylidenepyridylhydrazines: Synthesis, and kinetics and mechanism of their gas-phase pyrolysis [J]. Journal of Analytical and Applied Pyrolysis, 2017, 124: 446−453. DOI: 10.1016/j.jaap.2017.02.021.

[27] VLAEV L T, MARKOVSKA I G, LYUBCHEV L A. Non-isothermal kinetics of pyrolysis of rice husk [J]. Thermochimica Acta, 2003, 406(1−2): 1−7. DOI: 10.1016/S0040-6031(03)00222-3.

[28] LI Peng, YU Qing-bo, QIN Qin, et al. Kinetics of CO_2/coal gasification in molten blast furnace slag [J]. Industrial & Engineering Chemistry Research, 2012, 51(49): 15872−15883. DOI: 10.1021/ie301678s.

[29] BEURIA P C, BISWAL S K, MISHRA B K, et al. Study on kinetics of thermal decomposition of low LOI goethetic hematite iron ore [J]. International Journal of Mining Science and Technology, 2017, 27(6): 1031−1036. DOI: 10.1016/j.ijmst.2017.06.018.

[30] HE Kun, ZHANG Shui-chang, MI Jing-kui, et al. Pyrolysis involving n-hexadecane, water and minerals: Insight into the mechanisms and isotope fractionation for water-hydrocarbon reaction [J]. Journal of Analytical and Applied Pyrolysis, 2018, 130: 198−208. DOI: 10.1016/j.jaap.2018.01.009.

[31] LIU Hai-bo, SHU Dao-bing, SUN Fu-wei, et al. Effect of manganese substitution on the crystal structure and decomposition kinetics of siderite [J]. Journal of Thermal Analysis and Calorimetry, 2019, 136(3): 1315−1322. DOI: 10.1007/s10973-018-7767-9.

[32] LI Yan-jun, ZHANG Qi, YUAN Shuai, et al. High-efficiency extraction of iron from early iron tailings via the suspension roasting-magnetic separation [J]. Powder Technology, 2021, 379: 466−477. DOI: 10.1016/j.powtec.2020.10.005.

[33] CELIKDEMIR M, SARIKAYA M, DEPCI T, et al. Influence of microwave heating and thermal auxiliary on decomposition of siderite [J]. IOP Conference Series: Earth and Environmental Science, 2016, 44: 052002. DOI: 10.1088/1755-1315/44/5/052002.

[34] GHIMIRE S, DHO J. Anisotropic lattice disorder and enhanced magnetic anisotropy in Fe_3O_4 films on (110) $SrTiO_3$ [J]. Journal of Magnetism and Magnetic Materials, 2018, 468: 209−214. DOI: 10.1016/j.jmmm.2018.05.078.

[35] DHO J, KIM B, KI S. Substrate effects on in-plane magnetic anisotropy and verwey transition temperatures of (100) magnetite (Fe_3O_4) films [J]. IEEE Transactions on Magnetics, 2016, 52(7): 1−4. DOI: 10.1109/tmag.2016.2521604.

[36] ZHENG Yi-fan, LIU Hua-zhang, LIU Zong-jian, et al. In situ X-ray diffraction study of reduction processes of Fe_3O_4- and $Fe_{1-x}O$-based ammonia-synthesis catalysts [J]. Journal of Solid State Chemistry, 2009, 182(9): 2385−2391. DOI: 10.1016/j.jssc.2009.06.030.

[37] TOGAWA T, SANO T, WADA Y, et al. The effect of the crystal orientation on the rate of formation of cation-excess magnetite [J]. Solid State Ionics, 1996, 89(3−4): 279−286. DOI: 10.1016/0167-2738(96)00358-X.

[38] PONOMAR V P, BRIK O B, CHEREVKO Y I, et al. Kinetics of hematite to magnetite transformation by gaseous reduction at low concentration of carbon monoxide [J]. Chemical Engineering Research and Design, 2019, 148: 393−402. DOI: 10.1016/j.cherd.2019.06.019.

[39] YANG He, RONG Yi, HAN Chong, et al. Magnetizing roast and magnetic separation of iron in rare-earth tailings [J]. Journal of Central South University, 2016, 23(8): 1899−1905. DOI: 10.1007/s11771-016-3245-3.

[40] PONOMAR V P, DUDCHENKO N O, BRIK A B. Synthesis of magnetite powder from the mixture consisting of siderite and hematite iron ores [J]. Minerals Engineering, 2018, 122: 277−284. DOI: 10.1016/j.mineng.2018.04.018.

[41] PONOMAR V P. Thermomagnetic properties of the goethite transformation during high-temperature treatment [J]. Minerals Engineering, 2018, 127: 143−152. DOI: 10.1016/j.mineng.2018.08.016.

[42] YUNUS N A, ANI M H, SALLEH H M, et al. Effect of reduction roasting by using bio-char derived from empty fruit bunch on the magnetic properties of Malaysian iron ore [J]. International Journal of Minerals, Metallurgy, and Materials, 2014, 21(4): 326−330. DOI: 10.1007/s12613-014-0912-y.

(Edited by ZHENG Yu-tong)

中文导读

悬浮焙烧过程中菱铁矿热解原位动力学、相变及产物特性研究

摘要：菱铁矿是一种储量丰富的铁矿石，但其利用率较低，尚未得到高效开发利用。菱铁矿选择性转化为磁铁矿和CO是高效利用菱铁矿的关键。本文研究了悬浮磁化焙烧过程中菱铁矿的原位动力学和机理，丰富了菱铁矿作为还原剂的绿色悬浮磁化焙烧理论体系。气体产物分析表明，反应速率峰值随温度的升高而增大，且反应速率曲线呈现“早峰长尾”的特征。菱铁矿热解反应的机理模型为收缩球模型(R_3)：$f(\alpha)=3(1-\alpha)^{2/3}$，$E_\alpha$为46.4653 kJ/mol；$A$为0.5938 s^{-1}；动力学方程为$k=0.5938\exp[-46.4653/(RT)]$。原位HT-XRD结果表明，在$N_2$气氛下菱铁矿的最终产物为磁铁矿和方铁矿，它们具有良好结晶度。在620 °C时，固相产物的磁性达到峰值，其中饱和磁化强度(M_s)、剩磁磁化强度(M_r)和矫顽力(H_c)分别为53.63×10^{-3} A·m^2/g，10.23×10^{-3} A·m^2/g和12.40×10^3 A/m。经过焙烧，菱铁矿颗粒的致密结构遭到破坏，转变为疏松多孔的结构，降低了颗粒的力学强度，有利于降低后续磨矿作业的能耗。

关键词：菱铁矿；悬浮磁化焙烧；反应动力学；物相转化；磁性转变；微观结构演化